Optics Letters

Few-cycle 1.9-μm pulse generation via collinear spectrum synthesis in multiple-crystal OPA

Zuofei Hong,[1] Feilong Hu,[2] Xianglong Fu,[2] Wei Cao,[2] Qingbin Zhang,[2,*] and Peixiang Lu[1,2]

[1]Hubei Key Laboratory of Optical Information and Pattern Recognition, Wuhan Institute of Technology, Wuhan 430205, China
[2]School of Physics and Wuhan National Laboratory for Optoelectronics, Huazhong University of Science and Technology, Wuhan 430074, China
*Corresponding author: zhangqingbin@hust.edu.cn

Received 10 May 2019; revised 7 June 2019; accepted 12 June 2019; posted 12 June 2019 (Doc. ID 367303); published 8 July 2019

A multiple-crystal optical parametric amplification (OPA) design is reported for efficiently generating few-cycle 1.9-μm laser pulses. Different spectral regions of the idler pulse are successively amplified in three nonlinear crystals with delicately adjusted phase-matching angles, and a broadband spectrum supporting a three-cycle transform-limited (TL) pulse duration is obtained. Near-TL duration of 21.5 fs is realized by simple compression in a silicon window. Owing to sufficient exploitation of the pump energy in the crystals, total conversion efficiency of 31.3% is achieved with idler pulse energy of 65.8 μJ. The gain bandwidth in multiple-crystal OPA is markedly broadened compared to OPA using a single thick crystal; meanwhile, the high efficiency is preserved. Further energy scaling of the proposed scheme is potentially feasible using dual-chirped OPA geometry.

https://doi.org/10.1364/OL.44.003438

Energetic few-cycle laser pulses are powerful tools in multiple research fields. The ultrafast temporal resolution as well as high peak intensity can benefit studies including attosecond science [1], time-resolved spectroscopy [2], and nonlinear optics [3–5]. Compared to commercially available Ti:sapphire lasers, mid-infrared (mid-IR) femtosecond pulses can provide longer center wavelength, which is essential to numerous applications such as high-harmonic generation (HHG) [6] and strong-field ionization [7]. Even though extensive attention has focused on the generation of intense femtosecond pulses in the vicinity of 2 μm directly from a laser system [8,9], the compression of such pulses down to few-cycle duration has been restrained by the gain bandwidth of the laser medium.

Owing to the broadband gain and excellent tunability, optical parametric amplification (OPA) has become one of the most common sources of such pulses [10–12]. Few-cycle pulses around 2 μm have been produced using narrowband OPA accompanied by nonlinear spectral broadening in hollow-core fiber (HCF) or multiple thin plates [13–15]. Despite the versatility, spectral broadening inevitably reduces conversion efficiency and adds system complexity. The prerequisite for directly generating few-cycle pulses in OPA is a sufficient phase-matching bandwidth, which can be realized via quasi-phase matching (QPM) in periodically poled (PP) crystals [16–19]. However, the damage threshold of PP crystals is relatively low. Even though the possibility of power scaling using QPM is potentially enabled by large-aperture diffusion-bonded PP crystals [20,21], the validity of applying such crystals in various OPAs is yet to be confirmed. With the aim of multi-mJ pulse generation, bulk crystals with higher damage thresholds have been employed instead for scaling the system energy [22–24]. Limited by the phase-matching bandwidth in bulk crystal and the temporal shape of the pump pulse, the gain efficiencies for different parts of the signal/idler spectrum are not constant; the spectral bandwidth of the amplified pulse keeps getting narrower during amplification. The optimization of OPA usually involves reaching the balance between broad gain bandwidth and high conversion efficiency.

The gain-narrowing effect can be avoided by a chirp-compensation scheme, in which both the pump and seed pulses are chirped to realize phase matching for all temporal slices [25–27]. The performance of chirp compensation relies on the energy and bandwidth of the pump pulse, whereas the available pulse energy of the broadband pump is generally restricted by the damage threshold of the HCF or thin plates. In order to overcome the limit on the phase-matching bandwidth in a single crystal, several few-cycle pulses with a stabilized carrier–envelope phase (CEP) are generated from different OPAs and combined into a sub-cycle waveform [28,29]. The coherent synthesis opens new opportunities for ultrashort pulse generation, but the system can be quite complex with a high requirement on stability. Alternatively, instead of amplifying pulses in the time domain, the frequency-domain OPA (FOPA) was investigated in [30,31]. Four regions of the signal spectrum are spatially separated and recombined using a symmetrical $4-f$ setup, during which each region is amplified by a picosecond pump in four pieces of individually tuned nonlinear crystals. Although FOPA has been proven capable of simultaneously obtaining a broadband spectrum and high-efficiency gain, implementation of this scheme requires precise alignment of the input pulses.

In this Letter, we propose a novel design of broadband OPA for efficiently generating few-cycle pulses at 1.9 μm. Different regions of the spectrum are amplified in three beta-barium borate (BBO) crystals; the interacting pulses travel through the crystals without the need of separating and recombining

the laser beam, which significantly simplifies the experiment. The input pulses are slightly stretched to improve the overlap between interacting pulses, and the crystal angles are strategically adjusted to satisfy phase-matching conditions for each part of the idler spectrum. As a result, a broadband idler spectrum combining three spectral regions is obtained, and the pulse is easily compressible to near-transform-limited (TL) duration with only a silicon window. Moreover, the pump pulse is sufficiently depleted due to the large total crystal thickness, leading to high pump-to-idler conversion efficiency.

The experimental setup of the multiple-crystal OPA is presented in Fig. 1. A commercially available 800 nm, 25 fs, 1 mJ, 1 kHz Ti:sapphire laser is employed. The initial laser is split into three beams with pulse energies of 50 μJ (seed), 200 μJ (first stage pump), and 750 μJ (second stage pump), respectively. The 50 μJ beam is filtered by a variable density filter (VDF), and a pulse of ∼3 μJ is transmitted and focused into a 3 mm sapphire plate for white-light generation (WLG). The near-IR (NIR) portion of the white light is utilized as the seed source and pre-amplified by the first pump pulse in a 2.4 mm type-I BBO crystal cut at 20°. A small noncollinear angle (<1°) is used for separating the output pulses. Type-I crystal is utilized to maximize signal bandwidth; as a result, a 15 μJ signal pulse centered at 1400 nm with a full width at half-maximum (FWHM) bandwidth of over 300 nm is obtained and employed as the seed in the subsequent stage. The second pump beam is truncated with an aperture to utilize the most intense and homogeneous part in the spatial profile of the beam. Approximately 500 μJ beam energy is transmitted and utilized as the pump in the second stage.

The pump and seed beams are both collimated with a beam diameter of 5 mm, and they are combined with a dichroic mirror in a collinear geometry in the second stage, which consists of three pieces of type-II BBO crystals cut at $\theta = 27.0°$ and $\phi = 30°$ with thicknesses of 1 mm, 2 mm, and 3 mm, respectively. Note that the phase-matching angles of each crystal are slightly adjusted to 27.9°, 27.0°, and 26.6° to realize amplification for different parts of the spectrum. Type-II crystals instead of type-I are utilized owing to the higher nonlinearity and damage threshold, which is more beneficial for highly efficient amplification. In order to minimize the influence of the spatial walk-off of *e*-polarized pump and idler beams, the first and second crystals in the second stage are oriented in a way that the walk-off directions are opposite to each other. Consequently, the spatial walk-off in the two crystals can be cancelled out, ensuring good spatial overlap in the third crystal. The first crystal is selected with the least thickness owing to the highest pump intensity. As the amplification takes place, the pump pulse is depleted and the intensity decreases; thus, thicker crystals are required for the subsequent amplification to achieve similar intensity at different idler wavelengths. The output pump and signal pulses are removed by a long-pass filter, and a silicon window is used to compress the output idler pulse.

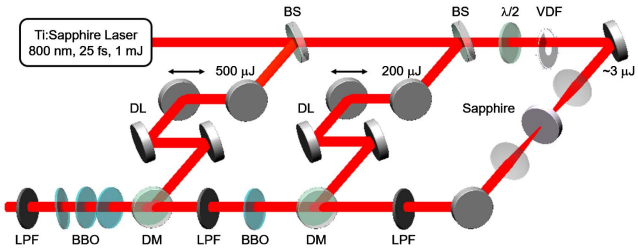

Fig. 1. Schematic setup of the system. BS, beam splitter; VDF, variable density filter; $\lambda/2$, half-wave plate; LPF, long-pass filter; DM, dichroic mirror; DL, delay line.

To begin with, we investigate the amplification in each individual BBO crystal. The phase-matching efficiencies $[\mathrm{sinc}(\Delta kL/2)^2]$ in the crystals are calculated and depicted in Figs. 2(a)–2(c). The figures show that the pump wavelength components between 750 nm and 850 nm are phase-matched to different idler wavelength components in each crystal when different angles are selected. Consequently, the experimentally obtained idler spectra from each crystal individually center at various wavelengths [Fig. 2(d)], with pulse energies of 9.0 μJ, 17.4 μJ, and 39.9 μJ, respectively. The input pump and seed parameters for each crystal are the same. It is observed that with a thicker crystal, the idler pulse is generated with higher energy and narrower bandwidth, which agrees with the gain-narrowing effect. However, by amplifying the idler pulse successively in all the above crystals, the larger crystal thickness will lead to higher conversion efficiency, and since different components of the idler spectrum are amplified in each crystal, a broader output spectrum can be expected as well.

Note that the longer wavelength components of the idler are amplified in the first crystal and the shorter wavelength components in the last crystal, which is based on the group delay (GD) between interacting pulses and the positive temporal chirp of the seed pulse. In the employed BBO crystals, the pump pulse propagates faster than the seed pulse. As the pulses travel inside the crystals, the pump pulse tends to move toward the leading edge of the seed pulse. Since the seed pulse is positively chirped, the trailing edge with shorter wavelength components is amplified first, and the leading edge is amplified last. Correspondingly, the longer wavelength components of the idler are amplified before the shorter wavelength components, leading to a negatively chirped idler pulse. On the contrary, if the long wavelength components (leading edge) of the seed pulse are amplified in the first crystal, the GD between the pulses will lead to a complete temporal walk-off and inhibit further amplification in the following crystals.

In our experiment, we employ a pump pulse of ∼60 fs, which is initially chirped inside the laser system without further

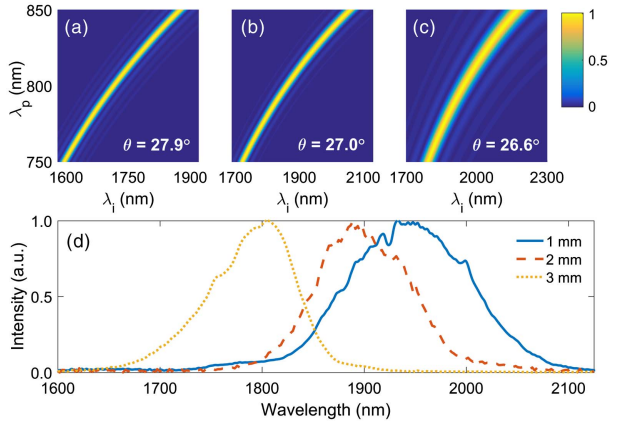

Fig. 2. Phase-matching efficiency with the crystal angles of 27.9° (a), 27.0° (b), and 26.6° (c). (d) Idler spectra obtained from individual BBO crystals of 1 mm (blue line), 2 mm (red dashed line), and 3 mm (yellow dotted line), respectively.

dispersion management. The pump duration is optimized as a balance between the gain bandwidth and conversion efficiency. The idler spectrum obtained in this condition is plotted in Fig. 3(a). The successive amplification in three crystals results in a broadband spectrum combining each individual spectrum, spanning 1600–2100 nm range with a FWHM bandwidth of 280 nm, which supports a three-cycle TL pulse duration of 19.1 fs. The output signal and idler pulse energies are 90.6 μJ and 65.8 μJ, respectively, corresponding to a total conversion efficiency of 31.3% and a pump-to-idler conversion efficiency of 13.2%. The energy stability of the idler pulse is recorded and plotted in Fig. 3(c), and the idler energy with a root-mean-square (RMS) fluctuation of 1.6% is obtained. After loosely focusing the idler beam, a circular spatial profile is observed at its focal point [Fig. 3(b)].

In comparison, the amplification in a piece of 6 mm bulk BBO crystal is investigated. The effective crystal thickness is the same as the three thin crystals combined, and the phase-matching angle is tuned to amplify the idler pulses centered at 2000 nm, 1900 nm, and 1800 nm, respectively. The obtained idler spectra are plotted as the blue, red, and yellow lines in Fig. 3(a), with the FWHM bandwidths and the pulse energies of 74 nm/71.9 μJ, 79 nm/73.9 μJ, and 95 nm/66.9 μJ, respectively. Using the same effective crystal thickness, the proposed scheme is able to produce idler pulses of slightly lower energy while much broader spectral bandwidth compared to the bulk crystal. The lower conversion efficiency results from the reflection on the crystal surfaces, which can be improved by using anti-reflection coating on the crystals.

The pulse duration is measured with a home-built frequency-resolved optical grating (FROG) device. The uncompressed idler pulse has a duration of 78.6 fs, longer than the pump pulse due to the temporal walk-off during amplification. Since the signal and idler pulses move toward opposite directions with respect to the pump in the studied condition, the pulses tend to stay within the pump pulse range and keep being amplified even when the crystal is longer than the pulse splitting length, which is another reason for selecting type-II crystals in this experiment.

A piece of 0.6 mm silicon window is utilized to compensate the negative chirp, and the plate is rotated to optimize its effective thickness. The results are presented in Fig. 4. It is noteworthy that the beam splitter (BS) used in FROG has a thickness of 3 mm, and the transmitted pulse is thus temporally stretched, whereas the reflected pulse remains unchanged. The difference between two pulses results in a slightly asymmetric FROG trace in Fig. 4(a), which is retrieved as cross-correlation FROG (XFROG) instead of second-harmonic generation (SHG)-FROG. The trace is retrieved with an error of 0.004, and the idler pulse with a near-TL duration of 21.5 fs is achieved, corresponding to 3.4 cycles. A flat temporal phase is observed in Fig. 4(c), indicating effective compensation of the dispersion. The idler CEP fluctuation is measured to be 496 mrad with a home-built $f-2f$ interferometer [Fig. 3(d)], which confirms the passive phase stabilization of the idler pulse.

Based on the above illustration, the GD between interacting pulses plays an important role during amplification. We have measured the idler spectra with varying pump-seed delays, and the results are plotted in Fig. 5. The "zero-delay" value is the condition that achieves the optimal idler spectrum (black line in Fig. 3), and a larger delay value indicates that the seed pulse propagates through a longer optical length, i.e., the pump pulse arrives at the crystal earlier. For the convenience of discussion, the spectrum regions amplified in 1 mm, 2 mm, and 3 mm BBO crystals will be referred to as R1 (short λ_s and long λ_i), R2, and R3, respectively. Since the signal is positively chirped, R1 is in the trailing edge of the pulse and R3 is in the leading edge.

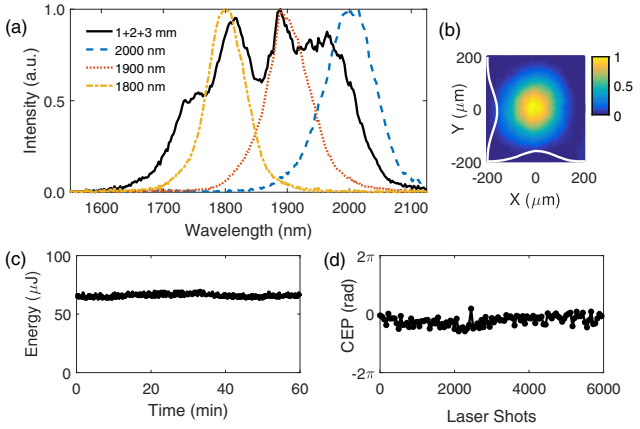

Fig. 3. (a) Idler spectra obtained from a 6 mm single crystal (blue, red, yellow) and multiple crystals (black). (b) Spatial profile of loosely focused idler beam. (c) Energy stability of the idler pulse. (d) CEP fluctuation of the idler pulse.

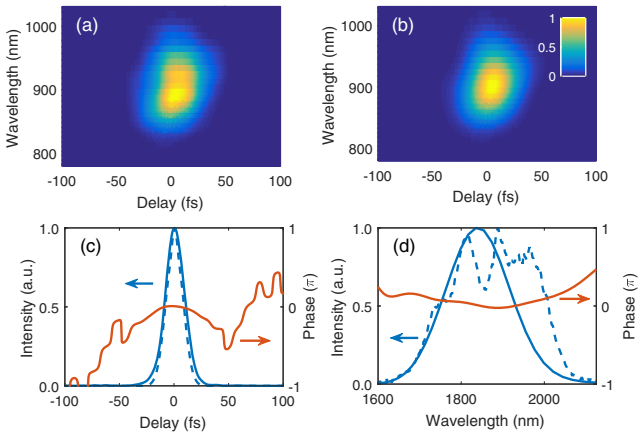

Fig. 4. (a) Measured FROG trace; (b) retrieved FROG trace; (c) temporal envelope (blue), phase (red), and TL pulse (blue dashed line); and (d) retrieved spectrum (blue), measured spectrum (blue dashed line), and phase (red) of the compressed idler pulse.

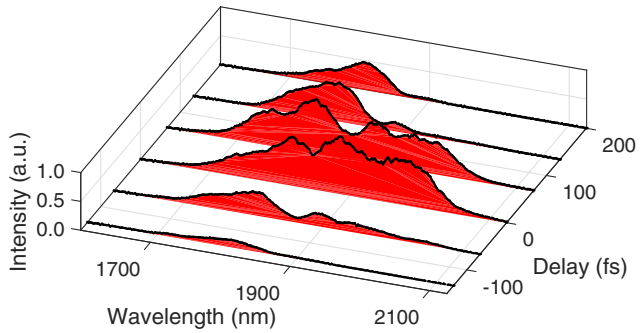

Fig. 5. Idler spectra with different pump-seed delay.

In the "zero-delay" case, the pump pulse actually reaches the first crystal later than the seed pulse and catches up in the successive crystals because of its larger group velocity. Due to the least crystal thickness in the beginning, the highest pump intensity is utilized to amplify R1; therefore, the pump peak overlaps with R1 in the first crystal. In the second and third crystals, the pump pulse moves faster than the seed and overlaps with R2 and R3, respectively. Even though the pump peak intensity keeps decreasing during amplification, the larger crystal thicknesses compensate the lower gain efficiency. In consequence, similar peak intensities are realized for all the regions, and the largest idler bandwidth is obtained.

By introducing a positive delay, the pump peak overlaps with R2 instead of R1, and a larger delay leads to its overlap with R3. As a result, R1 disappears suddenly between $\Delta t = 66$ fs and $\Delta t = 133$ fs due to the small crystal thickness and deteriorated overlap, whereas R2 weakens slower with the longer crystal. Last, R3 becomes dominant owing to its optimized overlap and largest crystal thickness; hence, a single peak spectrum at $\Delta t = 200$ fs is obtained. Oppositely, when a negative delay is introduced, the whole seed pulse is moved out of the pump pulse. R1 is barely amplified with insufficient crystal length, and R2 and R3 can still get amplification owing to the thicker crystals.

Despite the above illustrations, the significance of controlling the pulse delay can be markedly relaxed by combining the proposed scheme with the dual-chirped OPA (DC-OPA) [32]. When both the pump and seed pulses are stretched to picosecond level durations, the overlap between interacting pulses will be barely affected by the group delay. The performance instability resulting from the sensitive dependence on the pulse delay will therefore be eliminated. Meanwhile, when suitable crystals are selected, broadband phase matching can be achieved, and synthesis of the spectra obtained in each crystal is still valid. In this case, much higher pump energy can be utilized; the successive amplification in multiple crystals will still lead to high conversion efficiency, hence increasing the energy scalability of the multiple-crystal OPA.

To conclude, we present efficient generation of a few-cycle 1.9 μm pulse using a multiple-crystal OPA. Three different parts of the idler spectrum are successively amplified in three BBO crystals, each with an individually optimized phase-matching angle. The pump energy sufficiently converts to the signal and idler owing to the large crystal thickness. Total conversion efficiency of 31.3% and pump-to-idler efficiency of 13.2% are achieved. Meanwhile, the gain-narrowing effect in conventional single-crystal OPA is effectively overcome in multiple-crystal OPA, resulting in a significantly broadened idler spectrum with the FWHM bandwidth of 280 nm, and idler pulses with TL duration of three cycles are achieved. The idler pulse is simply compressed by a silicon window, resulting in a near-TL 3.4-cycle pulse duration of 21.5 fs. The interaction mechanism between the slightly chirped pulses have been investigated experimentally and discussed in detail. The multiple-crystal OPA scheme provides a simple and economic route of downconverting a commercially available Ti:sapphire laser to the mid-IR range, with few-cycle pulse durations, excellent conversion efficiency, and potentially high-energy scalability.

Funding. National Natural Science Foundation of China (NSFC) (11574101, 11627809, 11774111, 11804258).

REFERENCES

1. P. B. Corkum and F. Krausz, Nat. Phys. **3**, 381 (2007).
2. A. H. Zewail, J. Phys. Chem. A **104**, 5660 (2000).
3. A. Couairon and A. Mysyrowicz, Phys. Rep. **441**, 47 (2007).
4. D. M. Kinyua, H. Long, X. Xing, S. Njoroge, K. Wang, B. Wang, and P. Lu, Nanotechnology **30**, 305201 (2019).
5. D. Zhao, S. Ke, Y. Hu, B. Wang, and P. Lu, J. Opt. Soc. Am. B **36**, 1731 (2019).
6. L. Li, P. Lan, X. Zhu, T. Huang, Q. Zhang, M. Lein, and P. Lu, Phys. Rev. Lett. **122**, 193901 (2019).
7. J. Tan, Y. Zhou, M. He, Y. Chen, Q. Ke, J. Liang, X. Zhu, M. Li, and P. Lu, Phys. Rev. Lett. **121**, 253203 (2018).
8. X. Ren, L. H. Mach, Y. Yin, Y. Wang, and Z. Chang, Opt. Lett. **43**, 3381 (2018).
9. S. A. Rezvani, M. Suzuki, P. Malevich, C. Livache, J. V. de Montgolfier, Y. Nomura, N. Tsurumachi, A. Baltuška, and T. Fuji, Opt. Express **26**, 29460 (2018).
10. G. Cerullo and S. De Silvestri, Rev. Sci. Instrum. **74**, 1 (2003).
11. J. Biegert, P. K. Bates, and O. Chalus, IEEE J. Sel. Top. Quantum. Electron. **18**, 531 (2011).
12. Z. Hong, S. Rezvani, Q. Zhang, and P. Lu, Appl. Sci. **8**, 744 (2018).
13. C. Li, D. Wang, L. Song, J. Liu, P. Liu, C. Xu, Y. Leng, R. Li, and Z. Xu, Opt. Express **19**, 6783 (2011).
14. V. Cardin, N. Thiré, S. Beaulieu, V. Wanie, F. Légaré, and B. E. Schmidt, Appl. Phys. Lett. **107**, 181101 (2015).
15. R. Budriūnas, D. Kučinskas, and A. Varanavičius, Appl. Phys. B **123**, 212 (2017).
16. D. Brida, M. Marangoni, C. Manzoni, S. De Silvestri, and G. Cerullo, Opt. Lett. **33**, 2901 (2008).
17. X. Gu, G. Marcus, Y. Deng, T. Metzger, C. Teisset, N. Ishii, T. Fuji, A. Baltuska, R. Butkus, V. Pervak, H. Ishizuki, T. Taira, T. Kobayashi, R. Kienberger, and F. Krausz, Opt. Express **17**, 62 (2009).
18. J. Moses, S.-W. Huang, K.-H. Hong, O. D. Mücke, E. L. Falcão-Filho, A. Benedick, F. Ö. Ilday, A. Dergachev, J. A. Bolger, B. J. Eggleton, and F. X. Kärtner, Opt. Lett. **34**, 1639 (2009).
19. N. Bigler, J. Pupeikis, S. Hrisafov, L. Gallmann, C. R. Phillips, and U. Keller, Opt. Express **26**, 26750 (2018).
20. M. Missey, V. Dominic, L. Myers, and R. Eckardt, Opt. Lett. **23**, 664 (1998).
21. E. Sobolev, P. Komm, S. Noah, and G. Marcus, Opt. Lett. **44**, 1261 (2019).
22. Y. Deng, A. Schwarz, H. Fattahi, M. Ueffing, X. Gu, M. Ossiander, T. Metzger, V. Pervak, H. Ishizuki, T. Taira, T. Kobayashi, G. Marcus, F. Krausz, R. Kienberger, and N. Karpowicz, Opt. Lett. **37**, 4973 (2012).
23. K.-H. Hong, C.-J. Lai, J. P. Siqueira, P. Krogen, J. Moses, C.-L. Chang, G. J. Stein, L. E. Zapata, and F. X. Kärtner, Opt. Lett. **39**, 3145 (2014).
24. Z. Hong, S. A. Rezvani, Q. Zhang, and P. Lu, Opt. Quantum Electron. **49**, 392 (2017).
25. Y. Yin, J. Li, X. Ren, K. Zhao, Y. Wu, E. Cunningham, and Z. Chang, Opt. Lett. **41**, 1142 (2016).
26. Z. Hong, S. A. Rezvani, Q. Zhang, W. Cao, and P. Lu, Opt. Lett. **43**, 3706 (2018).
27. Z. Hong, Q. Zhang, S. A. Rezvani, P. Lan, and P. Lu, Opt. Laser Technol. **98**, 169 (2018).
28. S.-W. Huang, G. Cirmi, J. Moses, K.-H. Hong, S. Bhardwaj, J. R. Birge, L.-J. Chen, E. Li, B. J. Eggleton, G. Cerullo, and F. X. Kärtner, Nat. Photonics **5**, 475 (2011).
29. C. Manzoni, S.-W. Huang, G. Cirmi, P. Farinello, J. Moses, F. X. Kärtner, and G. Cerullo, Opt. Lett. **37**, 1880 (2012).
30. B. E. Schmidt, N. Thiré, M. Boivin, A. Laramée, F. Poitras, G. Lebrun, T. Ozaki, H. Ibrahim, and F. Légare, Nat. Commun. **5**, 3643 (2014).
31. P. Lassonde, N. Thiré, L. Arissian, G. Ernotte, F. Poitras, T. Ozaki, A. Laramée, M. Boivin, H. Ibrahim, F. Legaré, and B. E. Schmidt, IEEE J. Sel. Top. Quantum. Electron. **21**, 1 (2015).
32. Y. Fu, K. Midorikawa, and E. J. Takahashi, Sci. Rep. **8**, 7692 (2018).